Incident-Angle-Dependent Extraordinary Transmission of the Terahertz Bull's-Eye Structure

Yu Tokizane,[1,2,*] Seigo Ohno,[1,3,4] Yuma Takida,[1] Jun-ichi Shikata,[1,5] and Hiroaki Minamide[1]

[1] *Tera-Photonics Research Team, RIKEN Center for Advanced Photonics (RAP), RIKEN, Sendai 980-0845, Japan*

[2] *Institute of Post-LED Photonics, Tokushima University, Tokushima 770-8506, Japan*

[3] *Department of Physics, Graduate School of Science, Tohoku University, Sendai 980-8578, Japan*

[4] *Division for the Establishment of Frontier Sciences, Organization for Advanced Studies, Tohoku University, Sendai 980-8577, Japan*

[5] *College of Engineering, Nihon University, Koriyama 963-8642, Japan*

(Received 27 November 2021; revised 1 April 2022; accepted 5 April 2022; published 12 May 2022)

The bull's-eye structure in the terahertz (THz) frequency region has ample applications owing to its ability to focus free-propagating waves into subwavelength apertures, resulting in enhanced transmission, that is, extraordinary transmission. However, its coupling properties have been primarily discussed in terms of the normal plane-wave incidence to the structure. In this study, we investigate the multiple resonances in extraordinary transmission with normal and oblique incident waves. The experiment using a widely tunable and high-power THz wave source revealed two types of resonances. The main resonance split depends on the incident angle, and the other corresponds to the side lobe of the main resonances. The results are explained by a simple analytical model using a finite number of scattering media. The analysis is supported by the full-wave simulation using the finite-element method, which agrees with the experimental results. The coupling mechanisms will be applicable to design devices, such as THz biosensing devices or THz antennas for rapid communication systems.

DOI: 10.1103/PhysRevApplied.17.054020

I. INTRODUCTION

Surface plasmons (SPs) are collective oscillations of free electrons near the surface of metal or semiconductor materials. SP shows a local enhancement of electric fields at the subwavelength scale [1], which is applied to superresolution imaging [2] or miniaturization of electric circuits [3] to overcome the diffraction limit of the free propagating wave. Various experiments have demonstrated these properties in the wide wavelength range of electromagnetic waves from ultraviolet to microwave. In these experiments, the free-propagating wave excites SP with momentum matching using diffraction grating [4], periodic subwavelength hole arrays [5], or knife-edge structures [6].

The bull's-eye structure with concentric grooves around a single subwavelength aperture [7–16] is an attractive device that compensates for momentum mismatch to couple the SP and free-propagating wave. The aperture regenerates the SP as a tightly focused beam beyond the diffraction limit. The bull's-eye structure enhances the transmission by a few orders of magnitude compared with that from a single aperture without a structure. These properties are called extraordinary transmissions, which were found in the optical wavelength region [7]. They have also been verified in the millimeter wavelength and THz frequency region [8–15].

THz bull's-eye structure has garnered attention among researchers because of the following reasons. First, it has several applications, such as in THz superresolution imaging [13–15], where nondestructiveness and high spatial resolution are required simultaneously [17]. It is also applied to the THz high-gain antenna [9,11] for rapid wireless communication. Second, the THz bull's-eye device can be designed to be more compact than that in a millimeter wave, because the scale of the wavelength and period of the THz device is approximately a few hundred μm. Third, the THz wave has less diffraction or multireflection compared to that of the millimeter wave, which also makes the setup compact. Fourth, the propagation loss of the SP in THz frequency is smaller than that of SP in optical wavelength, which makes SP in THz frequency suitable for designing a device with a high Q factor. Fifth, a device

*tokizane@tokushima-u.ac.jp

with a scale of a few hundred μm allows precise microfabrication techniques, enabling precise comparison of the experiment and calculation.

Researchers have proposed the implementation of the normal incident THz wave in the bull's-eye structure to above applications. The THz-wave incidence with an arbitrary angle will provide further insights into the design of functional THz devices. In the optical wave or microwave bull's-eye structure, the oblique incidence was investigated experimentally [10,18] and numerically [19]. The reports revealed the angular robust coupling or angular sensitive spectral selectivity, which are useful in designing small antenna or spectral dispersive devices. These mechanisms are also useful for designing an angular robust THz antenna for rapid wireless communications or spectrally selective THz sensors for biosensing. However, the mechanism of the THz bull's-eye structure has not been investigated well, because precise THz spectra dependent on the incident angle were difficult to acquire due to the immature THz-wave sources and detectors in comparison to that of other frequency region. Thus, the applications were limited to using the normal incident THz wave around the resonant frequency, and the properties in the oblique incidence has been unrecognized.

In this study, we investigate the incident-angle-dependent extraordinary transmission of the THz bull's-eye structure experimentally, analytically, and numerically. We apply a high-power and widely tunable THz-wave source with a narrow linewidth to angle-dependent spectroscopy. The large dynamic range of the measurement revealed the angle-dependent shift and split of the transmission spectra along with the side lobes. By the simple analytical model, we determine the apparently complicated spectra are due to the interference of THz SP from periodic objects. The numerical simulation using the finite-element method reproduced the results, which supports analysis.

II. EXPERIMENTAL SETUP

To investigate the extraordinary transmission, we use the THz bull's-eye structure designed for the resonant frequency of the THz wave. Figure 1(a) shows a schematic of the bull's-eye structure positioned at the center of the stainless substrate. A circular aperture is at the center of the structure surrounded by a concentric grating on both surfaces of the substrate. The diameter of the aperture is smaller than the wavelength of the resonant THz wave. The period of the grating and the wavelength of the free-propagating wave are similar, which enables the free-propagating wave to couple the surface wave. Figure 1(b) depicts a side view of the cross-section structure along the dotted line in Fig. 1(a). The shape of the grating is rectangular, and the aspect ratio of the height and period is 1:10. The surface of the structure is coated with gold with a thickness of 1 μm, which is sufficiently thicker than the skin depth of the gold (approximately 0.1 μm). Thus, we regard this structure as the bulk of gold.

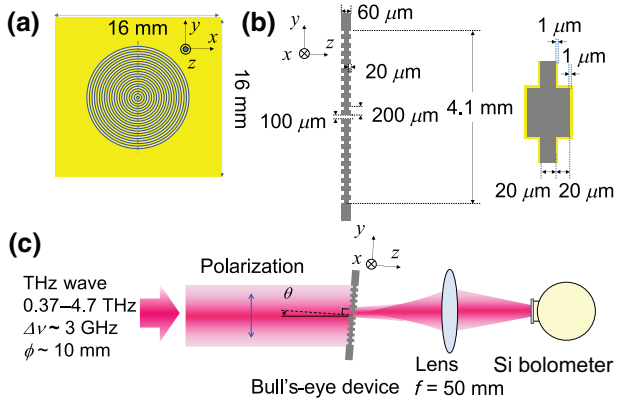

FIG. 1. Schematic of the bull's-eye structure (a) from top view and (b) side view at the cross section along the dotted line in (a). The structure is located on a center of a stainless substrate with 16×16 mm^2. Diameter of aperture size is 100 μm, the period of the concentric grating is 200 μm and the number of periods is 10. The height of grating is 20 μm and the thickness of the substrate is 60 μm at the maximum and 20 μm at the minimum. The inset shows the expanded structure, which shows a stainless substrate coated by a gold with a thickness of 1 μm. (c) Experimental setup to measure the transmission spectra as a function of incident angle. The THz wave is generated from the is-TPG source, which is tunable from 0.37–4.7 THz. θ is an angle of the bull's-eye rotation in y-z plane measured from the beam axis. Polarization is aligned vertical to the x axis. Polymer lens with focal length of 50 mm (PAX, Inc.) is used for collecting and focusing the transmitted beam to the Si bolometer (Infrared Laboratories, Inc.). The signal is acquired by the data-acquisition system (National instruments, Inc.) and personal computer (PC). Frequency of THz wave and angle of the device are controlled by the PC.

Figure 1(c) demonstrates the experimental setup used to measure the transmission spectra. To precisely measure the angle-dependent extraordinary transmission, the input wave must have a narrow linewidth and wide tunability. We apply an injection-seeded THz-wave parametric generator (is-TPG) [20] as a THz-wave source. The source has a high peak power of approximately 10 kW in the subnanosecond pulse, which allows the measurement of the signal with a large dynamic range. The linewidth is approximately 3 GHz with wide tunability [21], which is sufficient to measure the extraordinary transmission with a linewidth of approximately 100 GHz at 1.5 THz in the reported value of the same structure [13]. In the present experiment, we use the frequency range of 1.2–2.1 THz. To measure the angle-dependent spectra, the angle divergence of the beam must be eliminated. The beam is collimated with an M square of 1.1 [20]; the beam diameter is approximately 10 mm around the sample position, which corresponds to a Rayleigh length of 40 cm. Thus, the beam

has a sufficiently uniform wave vector around the structure. The incident angle is rotated setting the y-z plane as a plane of incidence. To change the angle, the sample is rotated by the rotational stage. The linear polarization parallel to the y-z plane is incident on the sample. We define $p(s)$ polarization as the polarization parallel (normal) to the y-z plane. The polymer lens collects and focuses the beam transmitted into a detector. The 4.2-K composite Si bolometer is used for the detector. To avoid the THz-wave absorption signature in the spectra, the water vapor in the experimental setup is purged with dry N_2 gas.

III. EXPERIMENTAL RESULTS

Figure 2 shows the transmission spectra of the bull's-eye structure at normal incidence. The main peak is measured at a frequency of 1.5 THz, and the absolute transmission is approximately 0.3%. The peak frequency is the same as the period of the grooves, and the spectrum shape is similar to that in previous reports [13]; thus, the measured peak is an extraordinary transmission. The FWHM of the peak is 50 GHz, which is narrower than 100 GHz in a previous report [13]. The bandwidth is determined by the parameters of the structures, including the geometry, period and number of grooves, thickness of the substrate, materials, or linewidth of the wave source. In the present experiment, the values of these parameters are equal to those in previous reports, except for the linewidth of the THz-wave source, which is approximately 3 GHz in the present experiment and approximately 50 GHz in a previous experiment [13]. The linewidth of the present setup is sufficiently narrower than the bandwidth of the resonance; thus, the result resolves the bandwidth of resonance in the extraordinary transmission. The geometrical parameters, such as aperture diameter, groove width and depth, and number of grooves, are interlinked to control the transmission properties [22]. The parameters in the device achieve the acceptable transmission and spectral width for the THz measurement.

Figure 3(a) shows the intensity of the transmission spectra based on the frequency and incident angle with a step of 0.1°. The color shows the intensity of the transmission on a log scale. The maximum signal-to-noise ratio of the measurement is over 22 dB. The main feature of the spectra is that the resonant frequency at 1.5 THz split and shift depending on the incident angle. The extraordinary transmission is sensitive to the incident angle, and its tolerance is 1.5°, which is defined by half width at half maximum. Another feature is the side lobes of the main resonances around 1.6–1.9 THz, whose peak intensities are approximately 10 dB lower than main resonances. The large dynamic range of the system using the is-TPG source enabled the measurement of the angle-dependent split of the resonance and side lobes in the spectra. The angle dispersion of the resonant frequency is only measured when

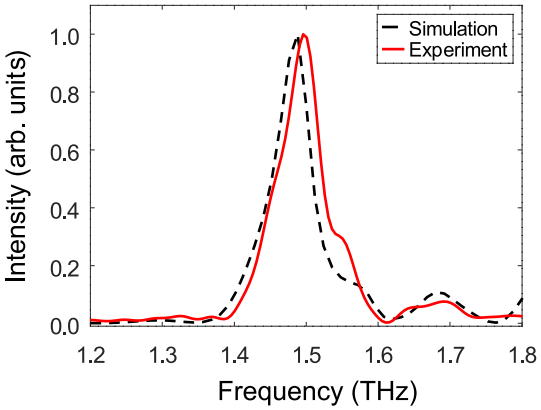

FIG. 2. Normalized transmission spectra of the bull's-eye structure with normal incidence. Red line shows experimental result and black dashed line shows the calculated result from FEM simulation.

the input wave is polarized parallel to the y-z plane and no dispersion is measured when the wave is polarized normal to the y-z plane. The SP is excited by both polarizations due to axially symmetric structure of the bull's-eye device. However, the SP principally distributes along the direction of input polarization, as the SP exists in TM modes. Thus, the angle dispersion is measured only when the SP distributes in the plane of incidence, where the input wave is p polarized. This anisotropic dispersion property is evidence of coupling between input wave and SP (see Appendix).

IV. ANALYTICAL MODEL

To analyze the angle dependence of the extraordinary transmission, we discuss the coupling of the SP and free-propagating THz waves by their dispersion relation. The wave-vector dispersion of SP on a flat metal material with a negative dielectric constant can be expressed as

$$k_{\mathrm{SP}}(\omega) = \frac{\omega}{c}\sqrt{\frac{\epsilon(\omega)}{1+\epsilon(\omega)}}. \tag{1}$$

Here, k_{SP} , ω, c, and ϵ are the wave number of the SP, optical angular frequency, speed of light, and dielectric constant of the material, respectively. To couple the SP to the free-propagating wave with a dispersion of $k_0(\omega) = \omega/c$, a structure to modulate the wave vectors, such as a grating structure, is required in the present experiment. The coupling condition in the modulated wave vector by the grating structure is expressed as

$$k_{\mathrm{SP}}(\omega) = k_0(\omega)\sin\theta + m\frac{2\pi}{\Lambda}, \tag{2}$$

where θ, Λ, and m denote the incident angle of the beam, period of the structure, and diffraction order, respectively.

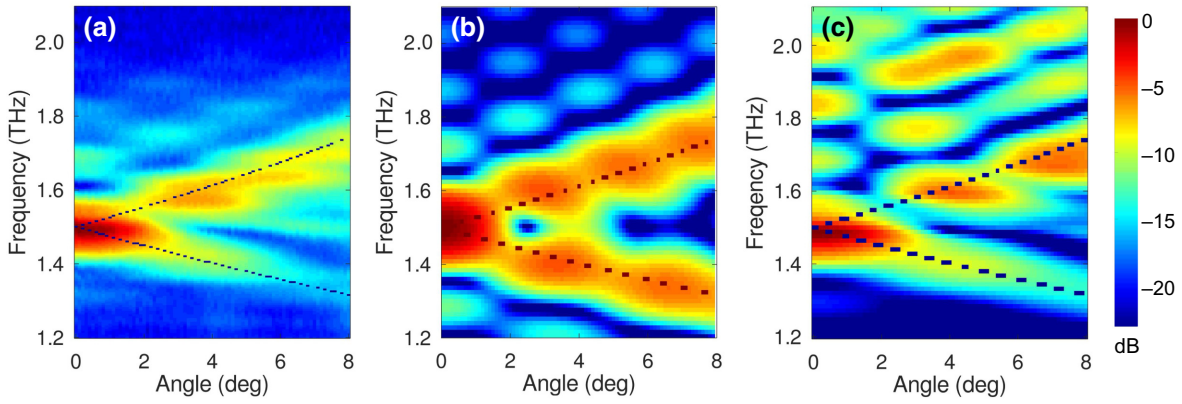

FIG. 3. Normalized transmission spectra of the bull's-eye structure mapped as a function of the angle and frequencies. (a) shows the experimental results. (b) shows the calculated results from the analytical model described by Eq. (3). (c) shows the results of the FEM simulation. The intensities are plotted in log scale. In the experiment, spectra are measured with an angle step of 0.1° from 0 to 8° and frequency interval of 5 GHz from 1.2 to 2.1 THz. In the analytical and numerical simulation, the angle step is 0.1° and frequency step is 12 GHz. The dotted lines are resonant frequencies calculated from Eq. (2).

The diffraction is expressed by the zone folding of the dispersion curve in the wave vector of $-\pi/\Lambda < k_{SP} < \pi/\Lambda$. The coupling frequency is tuned by the dispersion curve of the free-propagating wave, which is modulated by the incident angle θ. The dotted curves in Fig. 3(a) indicate the resonant frequencies calculated from Eqs. (1) and (2) with $m = +1$ and -1. The refractive index of Au in Ref. [23] is used to calculate $k_{SP}(\omega)$. The curves agree with the experimental results, which explains the split of resonances, where the first-order diffracted waves couple to the propagating SP modes that propagate in the $+x$ direction and $-x$ direction along the metal surface. The resonances degenerated at $k_{SP} = 0$, [$\theta = 0$ in Eq. (2)] and exhibited different frequencies at different wave numbers ($\theta \neq 0$). The angular dependence of the resonance is $\nu = c/\Lambda\sqrt{1/1 \pm \sin\theta}$, derived from Eq. (2), where the positive or negative sign corresponds to the lower or upper branch of the resonances. Figure 3(a) shows side-lobe resonances at around 1.6 to 1.9 THz as light blue spots ranging from 0° to 8°. The side lobes do not match the resonances described by Eq. (2). This indicates that the model oversimplifies the experiment assuming one-dimensional and infinite periods of grating.

To exclude infinite approximations from the model, we propose a simple analytical model using finite scattering media. Figure 4 presents a schematic of the model. The black dots denote the periodically arranged scattering media in one dimension, which represent the convex parts of the concentric grating along the cross section. The period of the media is $d = 200\ \mu$m, which is similar to that of the experiment. A plane wave is incident on the scattering media with an incident angle θ with p polarization. The incident wave arrives at each medium with a different optical path length. The wave scatters at the medium and propagates to the center position with path length Nd, corresponding to the distance from the Nth medium to the center position. The scattered waves from all media interfere at the center position and transmit the aperture as an extraordinary transmission. The combined wave at the center position can be expressed as

$$E = \sum_{N=1}^{10}\left[\exp[2\pi i\frac{Nd + c_0}{\lambda}(1 + \tan\theta)] + \exp[2\pi i\frac{Nd + c_0}{\lambda}(1 - \tan\theta)]\right], \tag{3}$$

where λ is the wavelength, and the first and second term represents the sum of the scattered waves propagating from the left and right side to the center. $Nd\tan\theta$ corresponds to the difference in the optical path length of the oblique plane wave at the Nth medium. c_0 is the offset

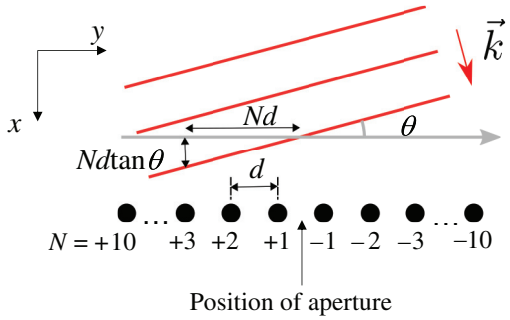

FIG. 4. Schematic of the analytical model using finite scattering media. Red lines show the wave front of the incident plane wave with p polarization. Black dots show the finite number of scattering media representing the convex part of the concentric gratings at the cross section. d is the period of the grating and θ is incident angle of the plane wave.

distance of the first scattering medium from the center position. The summation adds all scattered waves at the center position. The scattered waves have different initial phases and are enhanced in a constructive interference condition, resulting in extraordinary transmission. When the input wave is *s* polarized, the SP distributes perpendicular to the plane of incidence, then each medium acquires the same phase from the input wave irrespective to the incident angle, which results the angle independent resonance. The model includes the following assumptions for simplification. The model ignores the multiple scattering and concentric shapes of the grating. The scattering coefficient is constant, without wavelength dispersion.

Figure 3(b) demonstrates the intensity calculated from Eq. (3). The intensity is proportional to the square of the absolute value of the electric field. The results agree with the experimental results and the results obtained from Eq. (2) in the main resonant branches from 1.5 THz. The model also reproduced the side lobes of the resonances, which is not described by Eq. (2). Thus, the constructive interference condition in Eq. (3) explains the angle and frequency dependence of the side-lobe resonances. Furthermore, the model indicates that the constructive interference condition depends on the number of gratings N. To analyze the relationship between side-lobe frequencies and N, the transmission spectra are calculated with different numbers of periods using Eq. (3) for a normal incidence. We define the $\Delta\nu$ value as the difference frequency between the main peak (1.5 THz) and side lobe. The blue dots in Fig. 5(a) indicate that $\Delta\nu$ values are inversely proportional to the number of scattering media. The increase in the number of gratings will decrease $\Delta\nu$, which will converge to zero frequency that corresponds to the resonance of the infinite grating described by Eq. (2). These results show that a simple analytical model can facilitate a qualitative analysis of the experiment without significant numerical calculations.

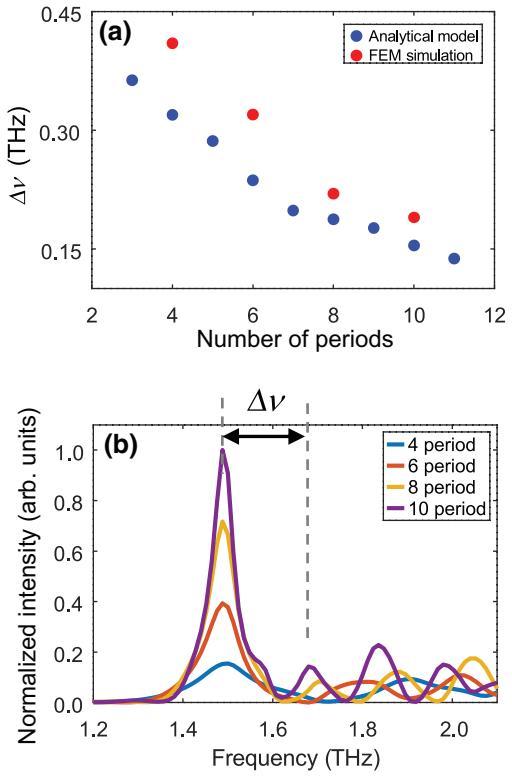

FIG. 5. (a) $\Delta\nu$ values as a function of the number of periods in normal incidence. $\Delta\nu$ is defined as a difference frequency between frequency at maximum intensity and that at next peak intensity. (b) Calculated transmission spectra of the bull's-eye structure with a period of 4, 6, 8, and 10 in normal incidence by FEM simulation.

V. NUMERICAL CALCULATION USING FINITE-ELEMENT METHOD (FEM)

To confirm the above discussion, we exclude one-dimensional approximations from the model and conduct a numerical calculation using a three-dimensional FEM simulation by employing a commercial software high-frequency structure simulator (HFSS, Ansys Inc.). In the simulation, the material of the bull's-eye structure is assumed to be a bulk of gold without frequency dispersion of the optical properties, because its dispersion is small in the THz frequency region. Figure 1(b) depicts the geometrical parameters used for the structures. The material parameter of gold is a conductive material with a conductivity of 4.1×10^7 S/m. A plane wave is incident with linear polarization simulated with a frequency interval of 12 GHz. The dashed curve in Fig. 2 indicates the transmission spectrum at a normal incidence. The results match with those of the experiment in terms of the frequency, spectrum width, and structure of the side lobe. The error of frequency is less than 1%, and the bandwidth matched within an error of 10%. The results accurately simulate the extraordinary transmission of the THz bull's-eye structure.

Similarly, the transmission spectra in the oblique incident wave are simulated. The parameters used in the simulation are the same as those used for the normal incidence [Fig. 1(b)]. The incident angle of the plane wave is varied from 0° to 8° by 0.1°. Figure 3(c) shows that the main resonance around 1.5 THz split and shift with increasing incident angle, which complies with the experimental results and analytical curves obtained by Eq. (2), as indicated by the dotted curves. In addition, the simulation results show the side lobes at around 1.6 THz to 1.9 THz whose frequencies and angle dependence are similar to the experimental results and analytical model from Eq. (3). No significant resonances, other than the main resonances, are calculated in the lower-frequency region. This nature also matches the experimental results, which are not reproduced by the analytical model. This low transmission

is owing to the cutoff frequency of the aperture, which is neglected by the analytical model.

To investigate the origin of the side lobes in the angle-dependent spectra, we investigate the relationship between the side-lobe frequencies and total number of gratings. Spectra are calculated in the normal incidence for simplicity. Figure 5(b) illustrates the transmission spectra from the FEM simulation with four different numbers of periods N ($N = 4, 6, 8$, and 10). The intensities are normalized to the maximum intensity of the structure with $N = 10$. The main resonant peaks have similar frequencies around 1.5 THz, but with different side-lobe frequencies: $\nu_{N=4} = 1.91$ THz, $\nu_{N=6} = 1.81$ THz, $\nu_{N=8} = 1.71$ THz, and $\nu_{N=10} = 1.68$ THz. The red dots in Fig. 5(a) depict the frequency difference $\Delta\nu$ between the main peak and subpeak as a function of N. The results have a similar dependence to that of the analytical model, represented by the blue dots in Fig. 5(a), which indicates the constructive interference of scattered waves in one dimension, explaining the side-lobe resonances. The validity of the simple analytical model also reveals that multiple scattering, including the cavity effect, is negligible in the THz bull's-eye structure because of the small coupling of SP in the THz frequency region compared to that of the optical region. The analytical model includes the normal and oblique incidence, which implies that the above principles hold in oblique incidence.

The spectra in Fig. 5(b) show that the peak intensities at 1.5 THz increase with an increase in number of periods. The intensities for N = 4, 6, 8, and 10 are 0.15, 0.39, 0.72, and 1.0, respectively. This enhancement indicates that an increasing number of scattering media increases the quantity of surface waves that contribute to the transmission. The results also exhibit bandwidth narrowing of the resonances. The values of Q factors, defined by $\delta\nu/\nu$, are 10, 16, 20, and 26 for N=4, 6, 8, and 10. Here, ν is the center frequency, and $\delta\nu$ is the FWHM of the resonance. The increase in the Q factor is similar in nature to the improvement of spectral resolution in the linear diffraction grating, where the resolution increases with the number of gratings. Based on these results, to increase the Q factor in the bull's-eye structure, a larger number of periods are required, and the input beam size must be optimized to cover the entire grating.

To visualize the distribution of surface waves along the structure, the amplitude of the electric field (E field) in four structures ($N = 4, 6, 8, 10$) are shown in Fig. 6 at the peak resonant frequencies in the normal incidence. The amplitude is plotted in the x-y plane near the input surface of the bull's-eye structure, and in the y-z plane across the aperture. The E field in x-y plane localizes within the concentric grating, whose area depends on the number of gratings. The localization reveals that the grating structure mediates the coupling between the incident wave and the SP. This coupling behavior originates the scattered waves, which are assumed in our analytical model described by Eq. (3). Thus, the area of the concentric grating determines the effective input beam size for the bull's-eye structure. The localized field distributes as a bowtie shape along the input polarization direction shown as a white arrow. The anisotropic profiles of the field distribution is evidence of the coupling between incident wave with linear polarization and SP, which exists in the TM mode. The results are contrasting to the coupling of the acoustic wave [16], which shows the axially symmetric coupling profile, because of the longitudinal wave property of the acoustic wave. The E field in y-z plane shows that the SP propagates and concentrates to the aperture along the input polarization direction, which contributes the extraordinary transmission from the aperture. In the structures with $N = 8$ and 10, the distribution of the E field has branches originating from the imperfection of boundaries in the FEM calculation. The imperfect boundary induces a reflecting wave with a rectangular-shaped wave front interfering with surface waves with a concentric wave front, resulting in these branch patterns, which is regarded as the artifact of the calculation.

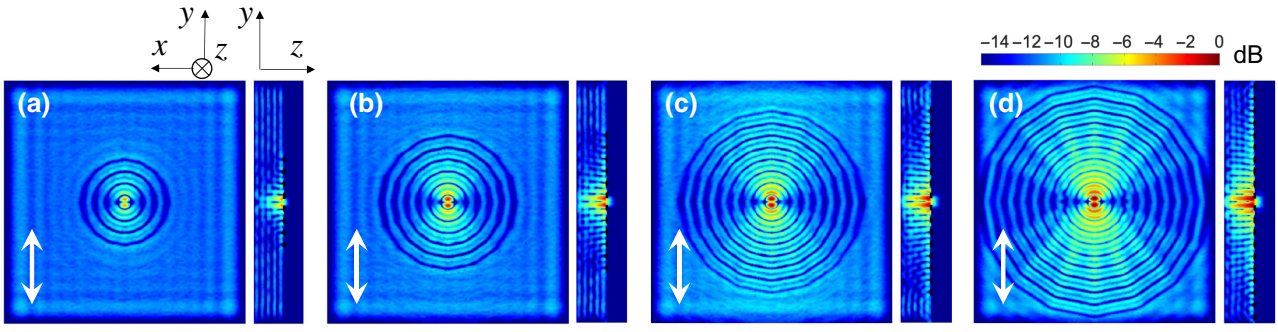

FIG. 6. Amplitude of electric field with a grating period of (a) 4, (b) 6, (c) 8, and (d) 10. The fields are calculated in a plane parallel to x-y plane located at 40 μm from the input surface of the bull's-eye structure (left), and in y-z plane across the aperture (right). The white arrow shows the polarization direction of the input wave.

The numerical simulation reproduces the experimental results and analytical calculation. The results reveal that the grating structure mediates the coupling between incident THz wave and SP. Finite number of gratings determines the coupling region and frequency of side lobes, which confirms the validity of the analytical model. The number of gratings increases the Q factor and makes the main and subresonances closer, and enhance the extraordinary transmission, whose mechanisms shed light on increasing the transmission of the THz bull's-eye structure.

VI. CONCLUSION

In this study, we investigate the angle-dependent transmission spectrum of the THz bull's-eye structure using an is-TPG in the frequency region of 1.2–2.1 THz with a 5-GHz step. The large dynamic range of the measurement revealed the angle-dependent split and shift of the resonant peak in the THz bull's-eye structure. The model based on diffraction theory explains the split and shift of resonances through coupling between the incident and surface waves. The proposed analytical model using finite scattering media revealed that the side lobes on the spectra is attributed to the interference of scattered waves, which are determined by the number of concentric gratings. This discussion is confirmed by three-dimensional FEM simulation. The simple model reveals the mechanism of directional coupling, which can be applied not only to design the THz superresolution imaging but also to design the intensity-enhanced THz antennas for beyond the 5G communication system, where an individual disregards the input beam divergence of monochromatic THz waves. The results will also be applied to design the spectrally selective THz biosensors or ranging applications to utilize directional coupling of THz waves.

ACKNOWLEDGMENTS

The authors acknowledge Professor H. Ito (RIKEN), Professor M. Kumano (Tohoku University), Professor T. Suzuki (National Institute of Technology, Sendai College), Dr. A. K. Dal Bosco, Dr. Z. Han (Hebrew University), Dr. Y. Moriguchi (RIKEN), Associate Professor T. Notake (Ishinomaki Senshu University), and Associate Professor K. Nawata (Tohoku Institute of Technology) for fruitful advice and discussions about the design of our research. We also thank researchers, technical staff, and members of the Tera-Photonics research team at RIKEN for great support. This work is supported by JSPS Grants-in-Aid for Scientific Research (No. JP19K05286, No. JP21K04928), JST A-STEP (No. JPMJTM20JX), RIKEN Science and Technology Hub Collaborative Research Program.

APPENDIX: INCIDENT ANGLE-DEPENDENT SPECTRA BY *S*- AND *P*-POLARIZED INCIDENT WAVE

Figure 7 shows the transmission spectra of the bull's-eye structure by three different incident angles θ with the polarization (a) normal and (b) parallel to the y-z plane. In our setup, the structure is rotated around the x axis to change the incident angle, then the spectra in (a) correspond to s-polarization input and that in (b) correspond to p-polarization input. The measurements are conducted using the experimental setup shown in Fig. 1. In the normal incidence, the results show the identical spectra in (a) and (b) due to the axial symmetry of the bull's-eye structure. In the oblique incidence, the resonant frequencies show no angle dispersion in (a) and show dispersion in (b). As the SP exists as TM mode, the SP principally distributes along the direction of input polarization. By the oblique incident wave, each grating structure acquires the same (different) phase when the SP distributes normally (parallel) to the plane of incidence. Thus, the resonant frequency has incident angle dispersion when the incident wave is

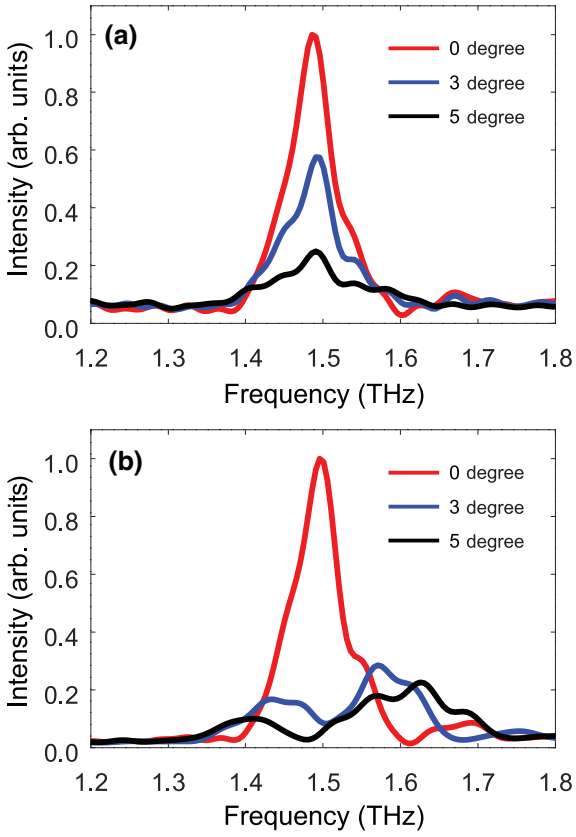

FIG. 7. The incident angle-dependent transmission spectra of the bull's-eye structure with (a) s-polarization and (b) p-polarization incidence. The red, blue, and black line shows the results with incident angle (θ) of 0, 3, and 5 degree. The spectra in (b) are extracted from Fig. 3(a).

p polarized. This anisotropic polarization dependence of spectra is evidence of the SP resonance.

[1] P. J. Schuck, D. P. Fromm, A. Sundaramurthy, G. S. Kino, and W. E. Moerner, Improving the Mismatch between Light and Nanoscale Objects with Gold Bowtie Nanoantennas, Phys. Rev. Lett. **94**, 017402 (2005).

[2] J. R. Krenn, A. Dereux, J. C. Weeber, E. Bourillot, Y. Lacroute, J. P. Goudonnet, G. Schider, W. Gotschy, A. Leitner, F. R. Aussenegg, and C. Girard, Squeezing the Optical Near-Field Zone by Plasmon Coupling of Metallic Nanoparticles, Phys. Rev. Lett. **82**, 2590 (1999).

[3] E. Ozbay, Plasmonics: Merging photonics and electronics at nanoscale dimensions, Science **311**, 189 (2006).

[4] R. H. Ritchie, E. Arakawa, J. Cowan, and R. Hamm, Surface-Plasmon Resonance Effect in Grating Diffraction, Phys. Rev. Lett. **21**, 1530 (1968).

[5] T. W. Ebbesen, H. J. Lezec, H. Ghaemi, T. Thio, and P. A. Wolff, Extraordinary optical transmission through sub-wavelength hole arrays, Nature **391**, 667 (1998).

[6] H.-T. Chen, R. Kersting, and G. C. Cho, Terahertz imaging with nanometer resolution, Appl. Phys. Lett. **83**, 3009 (2003).

[7] H. J. Lezec, A. Degiron, E. Devaux, R. Linke, L. Martin-Moreno, F. Garcia-Vidal, and T. Ebbesen, Beaming light from a subwavelength aperture, Science **297**, 820 (2002).

[8] C.-M. Chiu, H.-W. Chen, Y.-R. Huang, Y.-J. Hwang, W.-J. Lee, H.-Y. Huang, and C.-K. Sun, All-terahertz fiber-scanning near-field microscopy, Opt. Lett. **34**, 1084 (2009).

[9] U. Beaskoetxea, V. Pacheco-Peña, B. Orazbayev, T. Akalin, S. Maci, M. Navarro-Cía, and M. Beruete, 77-GHz high-gain bull's-eye antenna with sinusoidal profile, IEEE Antennas Wirel. Propag. Lett. **14**, 205 (2014).

[10] M. J. Lockyear, A. P. Hibbins, J. R. Sambles, and C. R. Lawrence, Surface-topography-induced enhanced transmission and directivity of microwave radiation through a subwavelength circular metal aperture, Appl. Phys. Lett. **84**, 2040 (2004).

[11] S. Ohno, Y. Tokizane, J.-i. Shikata, and H. Minamide, Phase and direction control of a terahertz wave propagating in a waveguide coupled with a bull's-eye structure, Ursi Radio Sci. Lett. **2**, 00 (2020).

[12] K. Ishihara, G. I. Hatakoshi, T. Ikari, H. Minamide, H. Ito, and K. Ohashi, Terahertz wave enhanced transmission through a single subwavelength aperture with periodic surface structures, Jpn. J. Appl. Phys., Part 2: Lett. **44**, L1005 (2005).

[13] K. Ishihara, K. Ohashi, T. Ikari, H. Minamide, H. Yokoyama, J.-i. Shikata, and H. Ito, Terahertz-wave near-field imaging with subwavelength resolution using surface-wave-assisted bow-tie aperture, Appl. Phys. Lett. **89**, 201120 (2006).

[14] T. Iguchi, T. Sugaya, and Y. Kawano, Silicon-immersed terahertz plasmonic structures, Appl. Phys. Lett. **110**, 151105 (2017).

[15] X. Deng, L. Li, M. Enomoto, and Y. Kawano, Continuously frequency-tuneable plasmonic structures for terahertz biosensing and spectroscopy, Sci. Rep. **9**, 3498 (2019).

[16] J. Mei, B. Hou, M. Ke, S. Peng, H. Jia, Z. Liu, J. Shi, W. Wen, and P. Sheng, Acoustic wave transmission through a bull's eye structure, Appl. Phys. Lett. **92**, 124106 (2008).

[17] D. M. Mittleman, Twenty years of terahertz imaging, Opt. Express **26**, 9417 (2018).

[18] M. S. Davis, W. Zhu, T. Xu, J. K. Lee, H. J. Lezec, and A. Agrawal, Aperiodic nanoplasmonic devices for directional colour filtering and sensing, Nat. Comm. **8**, 1347 (2017).

[19] A. Yamada and M. Terakawa, Reverse design of a bull's eye structure for oblique incidence and wider angular transmission efficiency, Appl. Opt. **54**, 3517 (2015).

[20] S. Hayashi, K. Nawata, T. Taira, J. Shikata, K. Kawase, and H. Minamide, Ultrabright continuously tunable terahertz-wave generation at room temperature, Sci. Rep. **4**, 5045 (2014).

[21] Y. Takida and H. Minamide, Frequency-domain spectroscopy using high-power tunable thz-wave sources: Towards THz sensing and detector sensitivity calibration, Proc. SPIE **10210**, 102100W (2017).

[22] O. Mahboub, S. C. Palacios, C. Genet, F. J. Garcia-Vidal, S. G. Rodrigo, L. Martin-Moreno, and T. W. Ebbesen, Optimization of bull's eye structures for transmission enhancement, Opt. Express **18**, 11292 (2010).

[23] M. A. Ordal, R. J. Bell, R. W. Alexander, L. L. Long, and M. R. Querry, Optical properties of fourteen metals in the infrared and far infrared: Al, Co, Cu, Au, Fe, Pb, Mo, Ni, Pd, Pt, Ag, Ti, V, and W, Appl. Opt. **24**, 4493 (1985).